#### **ORIGINAL PAPER**



# Negative sulfur-based electrodes and their application in battery cells: Dual-ion batteries as an example

Verena Küpers<sup>1</sup> · Martin Kolek<sup>1</sup> · Peter Bieker<sup>1,2</sup> · Marian Cristian Stan<sup>1</sup> · Tobias Placke<sup>1</sup> · Martin Winter<sup>1,2</sup>

Received: 12 May 2022 / Revised: 1 June 2022 / Accepted: 1 June 2022 / Published online: 17 June 2022 © The Author(s) 2022

#### **Abstract**

In this work, a cell concept comprising of an anion intercalating graphite-based positive electrode (cathode) and an elemental sulfur-based negative electrode (anode) is presented as a transition metal- and in a specific concept even Li-free cell setup using a Li-ion containing electrolyte or a Mg-ion containing electrolyte. The cell achieves discharge capacities of up to 37 mAh g<sup>-1</sup> and average discharge cell voltages of up to 1.9 V. With this setup, more than 100 cycles with a high capacity retention (>90% of the highest achieved value) and Coulombic efficiencies up to 95% could be achieved, which opens a broad new field for energy storage approaches.

**Keywords** Sulfur negative electrode · Dual-ion battery · Mg-ion battery · Transition metal-free, Li-free

### Introduction

The rising demand for energy storage based on an increasing market for electro mobility, drives the need for rechargeable batteries. While lithium ion batteries (LIBs) currently offer the best compromise between high energy, long lifetime, and safety, a foreseen shortage and cost increase of critical raw materials including lithium (Li), nickel and cobalt arise the need for alternative energy storage systems for certain applications [1–5]. This includes large-scale stationary storage systems, where cost (both for acquisition and for operation) is more important than energy density [3]. One transition-metal-free battery technology, which offers a high theoretical specific energy (2654 Wh kg $^{-1}$ ) is the sulfur  $\parallel$  Li metal battery (LSBs) [3, 6, 7]. However, challenges such as inhomogeneous electrodeposition and -dissolution of Li metal, as well as transport of soluble polysulfides (PSs) from

the sulfur-based positive electrode to the Li metal negative electrode and reactions thereof limit the Coulombic efficiency (C<sub>Eff</sub>) and cycle life of LSBs [6, 8-10]. Based on the comparably low potential of sulfur reduction and Li<sub>2</sub>S oxidation (≈2.2 V vs. Li|Li<sup>+</sup>), however, sulfur-based electrodes can also be considered as the negative electrode in combination with a high-potential positive electrode. In the past, several approaches combined negative electrodes based on elemental sulfur [11, 12] or sulfurized polyacrylonitrile (SPAN) [13–16] in combination with different positive electrodes ( $\approx 3.7$  to 4.1 V [17] vs. LiLi<sup>+</sup>) including LiMn<sub>2</sub>O<sub>4</sub> (LMO) [11, 13, 14], Na<sub>0.44</sub>MnO<sub>2</sub> [12], LiCoO<sub>2</sub> (LCO) [11], LiNi<sub>x</sub>Mn<sub>y</sub>Co<sub>z</sub>O<sub>2</sub> (NMC) [15] and anion intercalating graphite (4.0 to 4.6 V vs. LilLi<sup>+</sup>) [16], and achieved average discharge cell voltages between 1.5 and 2.0 V. Great advantages of sulfur as negative electrode are its high theoretical capacity (1672 mAh g<sup>-1</sup>) [6], low price (0.09 USD kg<sup>-1</sup>) [18] and potential sustainability (sulfur is a waste product of the petrochemical industry [19]). Furthermore, reductively less stable electrolytes including concentrated aqueous ones can be used [11, 15].

In this study a combination of a sulfur-based negative electrode with a high potential positive electrode based on anion intercalating graphite is presented [20]. In order to avoid confusion with sulfur | metal batteries, the terms positive electrode (P) for the anion intercalating graphite electrode with a higher potential and negative electrode (N) for the sulfur-based electrode with a lower potential will



Marian Cristian Stan marian.stan@uni-muenster.de

MEET Battery Research Center, Institute of Physical Chemistry, University of Münster, Corrensstraße 46, 48149 Münster, Germany

Helmholtz Institute Münster (HI MS), IEK-12, Forschungszentrum Jülich GmbH, Corrensstrasse 46, 48149 Münster, Germany

be used, instead of the terms 'cathode' and 'anode' [21]. A similar system containing a graphite P and a SPAN-based N was also presented by Shuai et al. in 2019, even though the theoretical capacity of SPAN is lower compared to the one of sulfur [16]. A schematic overview of the graphite || sulfur batteries in comparison to classical sulfur || metal batteries, including the expected electrode potentials and resulting discharge cell voltages is given in Fig. 1.

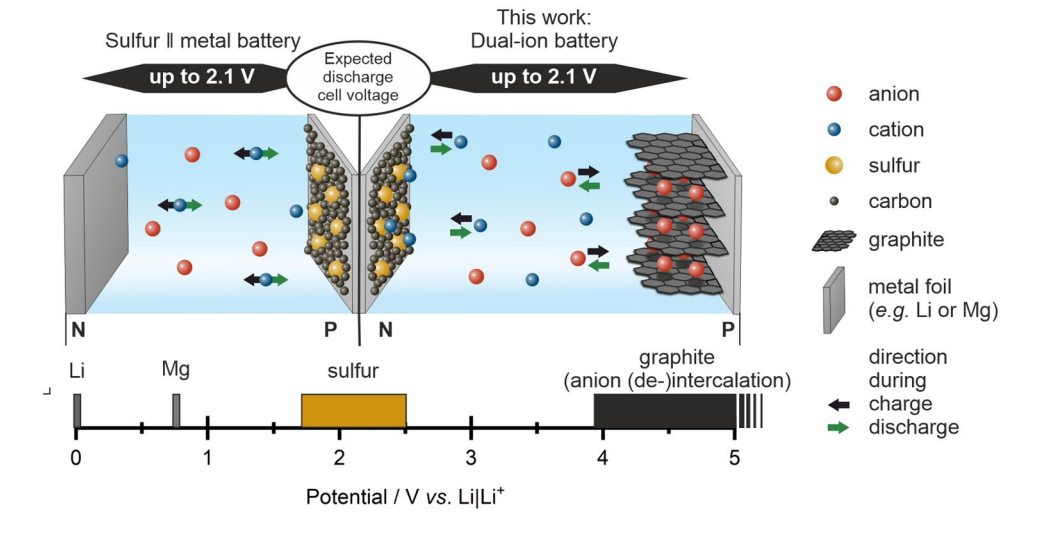
While in sulfur | metal batteries the cation is transported between the N and P during discharge and charge, in the dual-ion mechanism, both the cations and anions take part in the energy storage process [3]. During charge, the cations are stored in the N, while the anions are stored in the P, and released back into the electrolyte during discharge (indicated by black and green arrows in Fig. 1) [3]. As a result, the lithiation of the sulfur-based electrode, which is occurring during the discharge process in common LSBs, is occurring during charge in the presented graphite | sulfur system. Based on the high operating potential of the anion (de-)intercalation process (i.e., average deintercalation of TFSI<sup>-</sup> from graphite [22, 23]: ≈4.5 V vs. LilLi<sup>+</sup>), the expected average discharge cell voltage of graphite | sulfur cells is up to 2.1 V (average delithiation of sulfur [24, 25]: ≈2.4 V vs. LilLi<sup>+</sup>). This results in theoretical specific capacities of 129 mAh g<sup>-1</sup> and energy densities of 271 Wh kg<sup>-1</sup> (based on the active materials of P (graphite, 140 mAh g<sup>-1</sup>) and N (sulfur, 1671 mAh g<sup>-1</sup>) [22]). These values are comparable to the ones of lead acid batteries (120 mAh g<sup>-1</sup> and 245 Wh kg<sup>-1</sup> (based on the weight of lead (Pb) and PbO<sub>2</sub>), not including the weight of the electrolyte in both systems.

However, the high operating potential of anion intercalation into graphite limits the electrolytes to oxidatively stable ones, therefore, commonly ether-based electrolytes used in LSBs are not suitable [26, 27]. Furthermore in typical organic carbonate-based electrolytes [28], dissolved PSs tend to react with carbonate solvents [29] if the sulfur is

not trapped in microporous carbons or a polymeric composite (for example SPAN) [30], which might also occur in graphite | sulfur cells. One electrolyte system which is compatible with both sulfur-based electrodes as well as anion intercalation into graphite are the ones based on ionic liquids (ILs) [25, 31-34]. The performance of LSBs with selected IL-based electrolytes (e.g. with TFSI<sup>-</sup>-anions) was found to be improved, especially based on the low solubility of PSs in the electrolyte, reducing transport of the PSs to the N and subsequent reactions, which reduce the C<sub>Eff</sub> and cycle life in cells with high PS solubility [25]. However, a low solubility of PS in the electrolyte might lead to sluggish reaction kinetics, a poor rate capability and sulfur utilization, as well [35, 36]. 1 M lithium bis(trifluoromethanesulfonyl) imide (LiTFSI) in 1-butyl-1-methylpyrrolidinium bis(trifluoromethanesulfonyl)imide (Pyr<sub>14</sub>TFSI) was chosen as electrolyte for this study since it is well known for its good performance in dual-ion batteries (DIBs) [31–34, 37], as well as high capacity in LSBs (over 600 mAh g<sup>-1</sup>) [25].

Beside lithium-based electrolytes, the application of electrolytes with different cations including Na<sup>+</sup>, K<sup>+</sup>, Mg<sup>2+</sup> and Ca<sup>2+</sup> were used in both DIBs [37–43] and sulfur | metal systems [26, 44] (using sulfur-based Ps) and offer a great alternative to the critical raw material Li [1]. In order to evaluate, if graphite | sulfur cells can be used with various cations, graphite | sulfur cells with 0.5 M Mg(TFSI)<sub>2</sub> in Pyr<sub>14</sub>TFSI were studied exemplarily, as well. Mg-based batteries have attracted research in the past years, based on its high theoretical capacity, high abundancy [45] and an observed reduced tendency of Mg metal to form inhomogeneous electrodeposits compared to lithium metal [46–53]. Since the first rechargeable Mg battery, developed by Aurbach et al. in 2000 [54], efforts have been made to improve the performance of Mg-based batteries, including sulfur | Mg metal batteries (MSB) [6, 26, 55–57]. Similar to LSBs, however, most MSBs are based on ether-solvents

Fig. 1 Schematic overview of the cell setup used in this work (right) compared to the cell setup of a sulfur | metal battery (left), including an assignment of the electrodes to the expected electrode potentials and discharge cell voltages [22]. The positive electrode (P) and the negative electrode (N) of each system are labeled. The ion transport direction during charge and discharge are indicated by black and green arrows





[27, 37, 55, 58, 59]. MSBs containing electrolytes with only IL-based solvents, are to the best of our knowledge not vet known, even though MSBs with ether-IL mixtures showed good performances [61]. Different from Li-based DIBs, where Li metal or graphite were established as N, the incompatibility of most commonly used IL-based electrolytes (e.g. based on Pyr<sub>14</sub>TFSI) [62-66] to reversibly electrodeposit and -dissolve Mg metal limit Mg-ion-based DIBs to N with low or moderate specific capacities such as organic materials [40], Ti-Nb<sub>2</sub>O<sub>2</sub> nanoflakes [41] or activated carbon [37, 42]. Sulfur-based Ns for Mg-ion-based DIBs therefore offer a great alternative with a much higher specific capacity, even though the operating potential of the full cells is higher and thus the resulting cell voltage is lower. Still, graphite | sulfur cells with Mg-ion-based electrolytes are a transition-metaland Li-free system with highly abundant and low-cost active materials [3, 18, 45].

In this study, at first, the feasibility of graphite  $\parallel$  sulfur cells using ionic-liquid-based electrolytes is studied with a Li-ion-based electrolyte (1 M LiTFSI in Pyr<sub>14</sub>TFSI) at different currents and temperatures. In a second approach, the Li-ion-based electrolyte is exchanged with a Mg-ion-based one (0.5 M Mg(TFSI)<sub>2</sub> in Pyr<sub>14</sub>TFSI) to demonstrate the feasibility of this system as a transition-metal- and Li-free energy storage system.

# Results and discussion

# Graphite || sulfur dual-ion batteries using lithium-based electrolytes

The first investigated system is a graphite | sulfur cell with a 1 M LiTFSI in Pyr<sub>14</sub>TFSI (Li-Pyr) electrolyte. In order to differentiate between processes at the graphite-based working electrode (WE, higher operating potential, P in full-cells) and sulfur-based counter electrode (CE, lower operating potential, N in full-cells) and evaluate occurring processes, a three-electrode setup (half-cell setup [21], the potentials of both electrodes are monitored) with a Li metal reference electrode (RE) was used. As a starting point, the potentials of the graphite WEs were controlled (3.4 V and 4.9 V vs. LilLi<sup>+</sup>). In addition, the potential ranges of the sulfur CEs were limited to 1.5 and 3.0 V vs. LilLi<sup>+</sup> to avoid active material decomposition at the CE at low or high potentials. The specific discharge capacities (SDCs) and C<sub>Eff</sub>s at 100 mA g<sup>-1</sup>  $(g^{-1} = g^{-1}_{graphite})$  of graphite || sulfur cells are given in Fig. 2 and Table S3.

In comparison to graphite  $\|$  activated carbon (AC) cells [37], the SDCs are comparable (within  $33\pm 8$  mAh g<sup>-1</sup> after the  $10^{th}$  cycle), even though the  $C_{Eff}s$  are with  $41\pm 2\%$  (1st cycle) up to maximal  $95.8\pm 0.7\%$  ( $100^{th}$  cycle) notably lower (graphite  $\|$  AC:  $64\pm 2\%$  up to  $99.3\pm 0.2\%$  [37]). A lower  $C_{Eff}s$ 

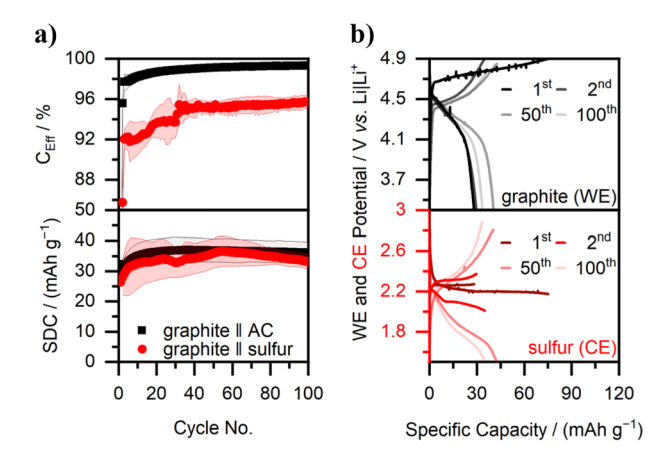


**Fig. 2** a  $C_{Eff}s$  and SDCs of graphite  $\parallel$  sulfur (WE  $\parallel$  CE; red) and graphite  $\parallel$  AC (WE  $\parallel$  CE; black, data taken from ref. [37], published under the terms of a CC BY 4.0 license, https://creativecommons.org/licenses/by/4.0/) Swagelok-type cells (three-electrode configuration, half-cell setup) with 1 M LiTFSI in Pyr<sub>14</sub>TFSI (Li-Pyr) electrolyte and a Li metal (LilLi<sup>+</sup>) RE at 20 °C, 100 mA g<sup>-1</sup> (10 mA g<sup>-1</sup> in the 1<sup>st</sup> cycle) and cut-off potentials of 3.4 and 4.9 V vs. LilLi<sup>+</sup> for the WE and additional limits of 1.5 and 3.0 V vs. LilLi<sup>+</sup> for the CE (only for the graphite  $\parallel$  sulfur cells). b The corresponding potential profiles of the WE (graphite, black) and CE (sulfur, red) at the 1<sup>st</sup>, 2<sup>nd</sup>, 50<sup>th</sup> and 100<sup>th</sup> cycle. The  $C_{Eff}s$  of the first cycle (CE=AC:  $64\pm2\%$  [37]; CE=sulfur:  $41\pm2\%$ ) are not shown.

when using a sulfur-based CE indicates more (irreversible) side reactions, which, however, does not seem to have a severe impact on the SDCs. One origin of these side reactions might be dissolved PSs in the electrolyte, which react (e.g. oxidation to elemental sulfur) at the high potentials of the graphite WE, similar to PS transport to the Li metal CE observed in in sulfur | metal cells [26, 67]. The presence of PS in the electrolyte (diluted in DME) even after one charge in graphite | sulfur cells was confirmed by UV/vis spectroscopy (Fig. S1) [68]. Furthermore, small defects on the surface of a (washed) WE could be obtained via scanning electron microscopy (SEM) after cycling in a graphite | sulfur cell which was not visible on a WE cycled in graphite | AC cells (Fig. 3a, b, defects are highlighted). Nevertheless, the sulfur content (in atomic %, at. %, detected by energy-dispersive X-ray spectroscopy, EDX) on the cycled WEs is independent of the CE  $(1.0 \pm 0.1 \text{ at. } \% \text{ vs. } 1.1 \pm 0.2 \text{ at. } \%$ , Table S1). The atomic % of elements detected by EDX, however, might vary since e.g. small amounts of remaining electrolyte on the sample can have an impact. Instead, the F:S elemental ratio can be more notable in order to elucidate elements present on the WE surface. The electrolyte, respectively the TFSI<sup>-</sup> anion, ideally has a F:S ratio of 3, while the pristine graphite WEs do not contain F or S (graphite, carbon black, CMC binder and Al current collector). The detected F:S ratio of the WE charged in a graphite | Li metal cell has a higher F:S ratio of 3.5:1, indicating a fluorine-rich



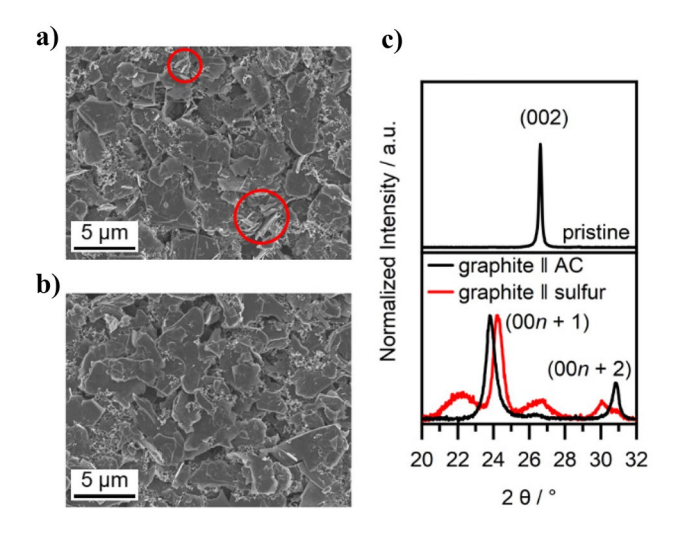


Fig. 3 SEM images (5000×magnification) of graphite WEs after three full cycles (3.4 to 4.9 V vs. LilLi+) and one charge to 4.9 V vs. LilLi<sup>+</sup> at 10 mA g<sup>-1</sup> in **a** graphite | sulfur (WE | CE) and **b** graphite | AC (WE | CE) Swagelok-type cells (three-electrode configuration, half-cell setup) with 1 M LiTFSI in Pyr14TFSI (Li-Pyr) electrolyte and a Li metal (LilLi+) RE at 20 °C. The SEM image of a pristine graphite electrode is given in Fig. S3a. c Normalized ex situ XRD patterns of pristine graphite electrodes (top, data taken from ref. [37], published under the terms of a CC BY 4.0 license, https:// creativecommons.org/licenses/by/4.0/) and graphite WEs after three full cycles (3.4 to 4.9 V vs. LilLi<sup>+</sup>) and one charge to 4.9 V vs. LilLi<sup>+</sup> at 10 mA g<sup>-1</sup> in graphite | sulfur (WE | CE; red) and graphite | AC (WE | CE; black, data taken from ref. [37], published under the terms of a CC BY 4.0 license, https://creativecommons.org/licenses/by/4.0/) Swagelok-type cells (three-electrode configuration, half-cell setup) with 1 M LiTFSI in Pyr<sub>14</sub>TFSI (Li-Pyr) electrolyte and a Li metal (LilLi+) RE

layer on the graphite, while the F:S elemental ratio is much lower in graphite | sulfur cells (1.8:1). This indicates a sulfur-rich layer on the graphite and reinforce the assumption of side reactions with dissolved PSs on the WE. The existence of a cathode electrolyte interphase (CEI) on positive graphite electrodes, however, is not yet clear [23]. No significant (permanent) interphase formation was for example observed on a positive graphite electrode after cycling with 4 M LiTFSI in EC/DEC, even though adsorbed anions were detected [69]. Further investigations are therefore needed to understand the different surface compositions on the graphite electrodes in detail. The potential profiles of the WE (Fig. 2b) are comparable to the ones observed in previous publications for TFSI-intercalation into graphite with LiTFSI in Pyr<sub>14</sub>TFSI electrolytes [23, 37, 60]: While an onset potential of  $\approx$ 4.6 to 4.7 V vs. LilLi<sup>+</sup> is visible in the first cycle, it is lowered to  $\approx 4.4 \text{ V vs. LilLi}^+$  in later cycles. Also, the specific differential capacity vs. potential plot of a graphite | sulfur cell is similar to the ones observed in graphite | AC cells [37] (Fig. S2). Only a small additional peak above 4.5 V vs. LilLi<sup>+</sup> during charge is visible, which is even

more pronounced at 10 mA g<sup>-1</sup> (Fig. S2b). Since no additional corresponding peak is observed during discharge, this peak might result from irreversible side reactions e.g., of dissolved sulfur species within the electrolyte, which are also reflected in the lower C<sub>Eff</sub> as discussed above (Fig. 2a). In order to elucidate, if the additional peak observed in the specific differential capacity vs. potential profiles results in more TFSI<sup>-</sup>-intercalation, or originates from (irreversible) side reactions, XRD measurements of cycled WEs were performed (Fig. 3c). In general, an increased intercalation of anions into graphite results in a lower staging number, visible in form of a larger splitting of the (00n + 1) and the (00n+2) reflections in XRD, respectively higher  $\frac{d_{(00n+2)}}{d_{(00n+1)}}$  ratio [37]. The application of a sulfur-based CE instead of an AC-based one results in a lower  $\frac{d_{(00n+2)}}{d_{(00n+1)}}$ , assuming the formation of stage III (CE = sulfur), instead of stage III to II (CE = AC) [33, 37], even though the specific charge capacity of the corresponding cells is with 52 mAh g<sup>-1</sup> much higher compared to 44 mAh  $g^{-1}$  (CE = AC) [37]. Therefore 8 mAh  $g^{-1}$ or more are likely lost by (irreversible) side reactions. Furthermore, one reflection at 26.6° indicates remaining graphite without intercalant for CE = sulfur. The additional reflection at 22.2° might arise from a shift of the (002) reflection of graphite, indicating a more amorphous structure, in good agreement with the slight alteration of the surface obtained via SEM (Fig. 3a) [70]. These results confirm the assumptions that the additional electrochemical activity at 4.6 V vs. LilLi<sup>+</sup> is not based on TFSI<sup>-</sup>-intercalation.

The potential of the CE in the first cycle (Fig. 2b) is comparable to the ones in previous studies of LSBs with long potential plateaus at  $\approx 2.2 \text{ V } vs. \text{ LilLi}^+$  (lithiation) and  $\approx$ 2.3 V vs. LilLi<sup>+</sup> (delithiation) [24, 25]. Since the cut-off potentials of the WE are reached during charge and discharge, before the potential limits of the CE are reached, the achieved capacities ( $\approx 65 \pm 8$  mAh g<sup>-1</sup> during charge and  $26 \pm 2$  mAh g<sup>-1</sup> during discharge) likely do not reflect the full achievable capacity of the N. Since the applied current is higher in the 2<sup>nd</sup> cycle, the potential hysteresis of the CE between charge and discharge increases (Fig. 2b) [25, 71]. In later cycles, the hysteresis increases even more, and starting approximately in the 50<sup>th</sup> cycle, the lower CE potential limit (1.5 V vs. Li|Li<sup>+</sup>) is reached during charge, before the upper WE cut-off potential (4.9 V vs. LilLi<sup>+</sup>) is reached, indicating an alteration of the CE. The increased overpotential of the CE, might arise from a loss of active material, for example by the dissolution of PSs into the electrolyte and reactions of these on the WE, as mentioned above (Fig. S1). Also the SEM image of a cycled sulfur CE contains hollow structures on the surface, not visible on the pristine electrode (Fig. S3b, c), and a reduced sulfur content  $(4 \pm 1)$  at. % vs.  $8 \pm 1$  at. %), indicating alteration of the CE, as well. As soon as the potential limit of the CE is reached, the charging



procedure is stopped and the subsequent discharge starts. Since the cut-off potential of the WE is not reached in this case, less TFSI<sup>-</sup> is intercalated into graphite in comparison to earlier cycles, decreasing the achievable specific charge capacity, which highly depends on the upper cut-off potential of the WE [33, 37]. Since less TFSI<sup>-</sup> is intercalated the subsequent SDCs are decreased, as well, which is observed by a slow fading of the SDCs starting approximately from the 50<sup>th</sup> cycle (Fig. 2a). In some identically built cells, also the upper CE potential limit (3 V vs. LilLi<sup>+</sup>) was reached, leading to an incomplete TFSI-deintercalation of the WE and TFSI<sup>-</sup>-accumulation within the graphite. This behavior was described by the electron and ion couple inventory model [72], where an uneven ion storage on either side leads to fading cell capacities. Besides reduced SDCs in later cycles, these performances decrease the average discharge cell voltages  $(E_{WE} - E_{CE}, E = \text{potential})$  from  $1.89 \pm 0.02$  V in the  $2^{\text{nd}}$ cycle to  $1.8 \pm 0.1$  V in the  $100^{th}$  cycle.

When the potential of CE is not additionally fixed in the potential range of 1.5-3.0 V vs. LilLi<sup>+</sup> (Fig. S4), the WE can be charged and discharged between 3.4 and 4.9 V vs. LilLi<sup>+</sup> in each cycle, resulting in slightly higher SDCs, also after the  $50^{\text{th}}$  cycle. Still, a slight fade of the SDCs for later cycles is observed, indicating alteration of the WE as well. In addition the potential profiles of the CE (Fig. S4b) reveal that potentials of  $\approx 1.2 \text{ V}$  vs. LilLi<sup>+</sup> during charge and  $\approx 3.4 \text{ V}$  vs. LilLi<sup>+</sup> during discharge are reached upon cycling, resulting in low cell voltages (*e.g.*, 0 V during discharge).

In a cell voltage controlled graphite  $\|$  sulfur cell (1 to 2.8 V, two-electrode setup), SDCs up to 29 mAh g<sup>-1</sup> with average discharge voltages of 1.9 V ( $\approx$ 55 Wh kg<sup>-1</sup>) were achieved at 100 mA g<sup>-1</sup> (Fi. S5), which is comparable to lead acid batteries [73]. However, the SDC decreased notably upon cycling, likely based on the increasing overpotential at the sulfur electrode, as observed in three-electrode cell configuration (Fig. 2b).

To evaluate, if the performance of graphite  $\|$  sulfur cells can be improved at different cycling conditions, the performance at different specific charge/discharge currents was evaluated. Previous studies showed that the SDCs of graphite  $\|$  AC cells increase at low, but decrease at high currents, while the  $C_{Eff}s$  change vice versa (Fig. 4a ) [37]. A similar trend can be observed in graphite  $\|$  sulfur cells, even though the SDC fading at high currents and the reduced  $C_{Eff}$  at low currents are more severe (Fig. 4a and Table S4).

The main origin of the low SDCs at high currents is based on increasing overpotentials of the sulfur CE, as visible in Fig. 4b, in good agreement with previous observations of electrochemical sulfur reduction and oxidation at high currents in LSBs containing IL-based electrolytes [25]. Especially at 1000 mA g<sup>-1</sup>, however, also the overpotential of the graphite WE is increased as also observed in graphite || AC cells [37], even though the potential limit of the CE

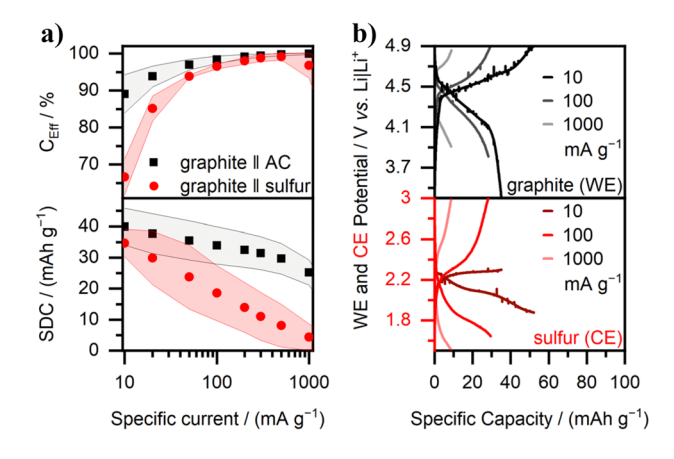
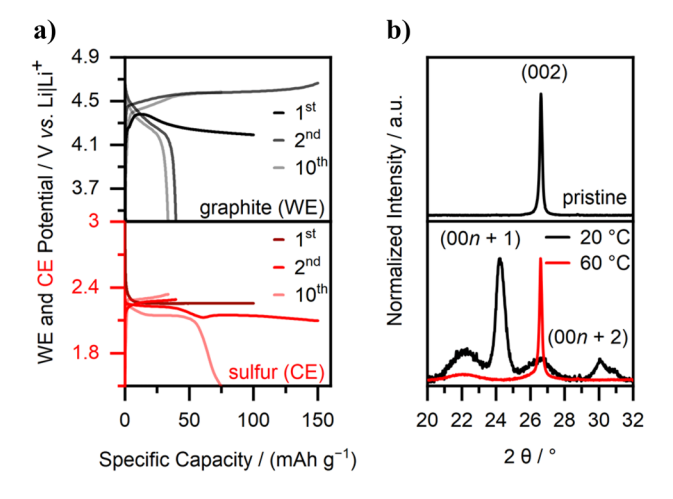


Fig. 4 a  $C_{\rm Eff}$ s and SDCs of graphite | sulfur (WE | CE; red) and graphite | AC (WE | CE; black, data taken from ref. [37], published under the terms of a CC BY 4.0 license, https://creativecommons.org/licenses/by/4.0/) Swagelok-type cells (three-electrode configuration, half-cell setup) with 1 M LiTFSI in Pyr<sub>14</sub>TFSI (Li-Pyr) electrolyte and a Li metal (Li|Li<sup>+</sup>) RE at various specific currents. The cut-off potentials at all currents were fixed to 3.4 and 4.9 V vs. Li|Li<sup>+</sup> for the WE and additionally limited to 1.5 and 3.0 V vs. Li|Li<sup>+</sup> for the CE (only for the graphite | sulfur cells). b The corresponding potential profiles of the WE (graphite) and CE (sulfur) at 10, 100 and 1000 mA g<sup>-1</sup>

is reached before the cut-off potential of the WE. The lower C<sub>Eff</sub>s at low currents was mainly attributed to a facilitated decomposition of the electrolyte and intercalated TFSI-, e.g., in graphite | AC cells [23, 37]. In graphite | sulfur cells, however, the transport of dissolved sulfur species towards the graphite WE and reactions thereof might be reinforced at lower currents, as well. For graphite | sulfur cells with no potential limit of the CE, the SDCs at different specific currents are comparable or even slightly higher compared to the values of graphite | AC cells [37], even though the C<sub>Eff</sub>s at low currents are lower, comparable to the cells with potential limited CE (compare Fig. S6a). This indicates that only sluggish reaction kinetics of the sulfur CE, but not dissolved sulfur species in the electrolyte are responsible for the reduced SDCs at high specific currents, while the lower C<sub>Eff</sub> indeed is controlled by sulfur-species.

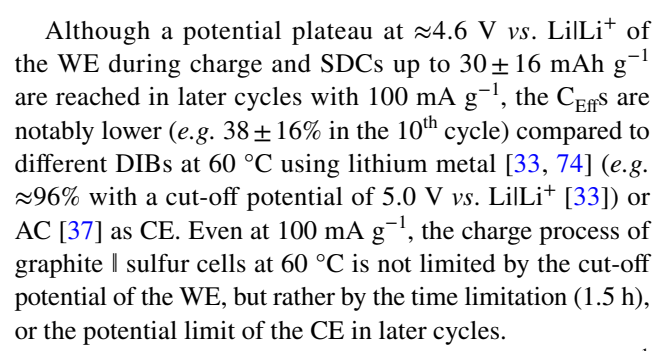
Previous, studies of LSBs [25] and different DIB systems [33, 34, 37, 74, 75] showed, that the sluggish reaction kinetics and high overpotentials (especially at high currents) can be reduced at elevated temperatures, improving the SDCs, even though the  $C_{Eff}$ S were slightly reduced, as well. In graphite | sulfur cells at 60 °C, however, the cycling performance is decreased notably compared to cells cycled at 20 °C (Fig. 5a and Table S3). Even though flat potential plateaus and low overpotentials ( $\approx$ 2.25 V vs. LilLi<sup>+</sup>) indicate an improved performance of the CE in the first cycles, the corresponding potential of the WE, is with 4.1 to 4.4 V vs. LilLi<sup>+</sup> lower compared to previous reports which usually show potentials above 4.4 V vs. LilLi<sup>+</sup> at 60 °C [74]. Furthermore, the first charge





**Fig. 5** a Potential profiles of the WE (graphite, black) and CE (sulfur, red) at the 1<sup>st</sup>, 2<sup>nd</sup> and 10<sup>th</sup> cycle of graphite | sulfur Swagelok-type cells (three-electrode configuration, half-cell setup) with 1 M LiTFSI in Pyr<sub>14</sub>TFSI (Li-Pyr) electrolyte and a Li metal (LilLi<sup>+</sup>) RE at 60 °C, 100 mA g<sup>-1</sup> and with cut-off potentials of 3.4 and 4.9 V *vs.* LilLi<sup>+</sup> for the WE and additional limits of 1.5 and 3.0 V *vs.* LilLi<sup>+</sup> for the CE. **b** Normalized ex situ patterns of pristine graphite electrodes (top, data taken from ref. [37], published under the terms of a CC BY 4.0 license, https://creativecommons.org/licenses/by/4.0/) and after three full cycles (3.4 to 4.9 V *vs.* LilLi<sup>+</sup>) and one charge to 4.9 V *vs.* LilLi<sup>+</sup> at 20 °C (black) and 60 °C (red) and 10 mA g<sup>-1</sup> in graphite | sulfur Swagelok-type cells with 1 M LiTFSI in Pyr<sub>14</sub>TFSI (Li-Pyr) electrolyte and a Li metal (LilLi<sup>+</sup>) reference electrode. In addition to the cut-off potentials a time limitation of 10 h (1<sup>st</sup> cycle) or 1.5 h (following cycles) per step was applied.

process is not limited by the cut-off potential of the WE, but time restrictions (10 h). One origin of the low overpotentials of the CE might be a higher solubility of sulfur species at elevated temperatures, which might improve its reaction kinetics, but enhance transport of PSs to the WE, as well [25, 36, 71]. The SDC of the first cycle is almost zero, which confirms that not TFSI<sup>-</sup>-intercalation, but (irreversible) side reactions occur at 4.1 to 4.4 V vs. LilLi<sup>+</sup>. Schmuelling et al. [33] found that electrolyte decomposition takes place above 5.1 V vs. LilLi<sup>+</sup> in graphite || Li metal DIBs with LiTFSI in Pyr<sub>14</sub>TFSI at 50 mA g<sup>-1</sup> and 60 °C. Still, a dominant stage I could be observed via XRD in graphite | Li metal cells at 60 °C [33]. In graphite | sulfur cells, however, the absence of TFSI<sup>-</sup>-intercalation (at 10 mAh g<sup>-1</sup>) could also be confirmed using XRD: Different from the electrode collected from a cell cycled at 20 °C, the electrode cycled at 60 °C shows only the reflection at 26.6°, as also observed for pristine graphite electrodes (Fig. 5b), and a weak reflection at 22.2°, which might originate from amorphous (002) carbon [70]. This indicates, that the observed irreversible side reactions in graphite | sulfur cells take place at notably lower potentials compared to graphite | Li metal cells, thus not electrolyte or electrode decomposition processes, but rather reactions of dissolved PSs are the main cause for the low C<sub>Eff</sub>s.



The overpotential of the CE remains low at 100 mA g<sup>-1</sup> (e.g. 2<sup>nd</sup> cycle, Fig. 5a), nevertheless, shorter plateaus of the CE in later cycles indicate a loss of active material (sulfur). Such a loss is likely originating from: i) irreversible side reactions of dissolved sulfur species that might reduce the amount of accessible sulfur species in the cell and ii) the electron and ion inventory effect [72] of the WE and CE. While during charge, low kinetic hindrances allow for sulfur reduction at the CE until the time limit is reached (high charge capacity), the re-oxidation of sulfur species is limited by the deintercalation of TFSI- (low discharge capacity based on a low C<sub>Eff</sub>). Thereby, large amounts of sulfur species are either lost (irreversible side reactions on the WE), or trapped in form of reduced species in the electrolyte or for example as solid Li<sub>2</sub>S on the CE. The accumulated capacity losses over the first 10 cycles are with more the  $2000~\text{mAh}~\text{g}^{-1}_{~sulfur}$  even higher than the theoretical capacity of the  $S^0$  to  $S^{2-}$  reduction.

In conclusion, elevated temperatures are not suitable to improve the performance of graphite  $\mathbb{I}$  sulfur cells. Even though elevated temperatures might improve the reaction kinetics of sulfur redox reactions of the CE [25], likely a higher solubility of PSs, reinforced transport of sulfur species to the WE and accordingly more severe irreversible side reaction on the WE, occurring at potentials below the TFSI^-intercalation reduce the  $C_{\rm Eff}$  notably.

Alternative modifications of graphite | sulfur cells might include different electrolyte compositions and amounts (especially the electrolyte:sulfur ratio) to tailor the viscosity, electrode wettability and PS solubility [76], which could have an impact on cycling performance. Especially the PS solubility is a key factor for the performance of sulfur-based electrodes: Even though a high PS solubility might improve the reaction kinetics of sulfur-based electrodes, it is known to cause transport of PSs to the CE (e.g. Li metal) in LSBs [25, 35, 36], respectively WE (graphite) in graphite | sulfur cells, reducing its C<sub>Eff</sub> and cycle life. For DIBs, however, a high oxidative stability of the electrolyte as present in ionic liquids [34, 37, 60] or highly concentrated [37, 77, 78] electrolytes is needed, as well. Highly concentrated carbonatebased electrolytes, however, might react with dissolved PSs [29], unless the sulfur is immobilized e.g. in microporous carbons or a polymeric composite [30]. A graphite | sulfur



cell, with a SPAN-based N and a 4 M LiPF<sub>6</sub> in ethyl methyl carbonate electrolyte for example showed a stable cycling performance [16]. The oxidative stability of highly concentrated ether-based electrolytes is too low and results in irreversible side reactions and low  $C_{Eff}s$  (Fig. S7). Trapping of dissolved PSs in the sulfur-based electrode [79] or the separator [80, 81] could therefore help to improve the performance of graphite  $\parallel$  sulfur cells, as well [6].

# Graphite || sulfur dual-ion batteries using magnesium-based electrolytes

In a second approach, a transition-metal- and Li-free cell system, using graphite  $\mathbb I$  sulfur cells with a Mg-ion-based electrolyte (0.5 M Mg(TFSI)\_2 in Pyr\_14TFSI, Mg-Pyr) is studied. While no notable differences of the TFSI^-intercalation into graphite could be observed when using Mg-Pyr instead of Li-Pyr in graphite  $\mathbb I$  AC cells [37], overpotentials of sulfur  $\mathbb I$  Mg metal batteries (MSBs) are usually higher compared to the ones observed in LSBs [82]. Beside higher overpotentials of Mg electrodeposition and -dissolution [82], which is not relevant for graphite  $\mathbb I$  sulfur cells, also an increased overpotential for the redox reactions of sulfur, respectively dissolved sulfur-species could be observed, based on different PS stabilization by Mg^2+ and Li^+ [68, 76]. This leads to different reaction mechanisms for sulfur oxidation and reduction and is solvent-dependent, as well [68, 76].

Since a potential shift of 0.1 V was observed for lithium metal (quasi-)reference electrodes for Mg-Pyr compared to Li-Pyr, the cut-off potentials were adapted to 3.4 V and 5.0 V vs. LilLi<sup>+</sup> for the WE and 1.6 V and 3.1 V vs. LilLi<sup>+</sup> for the CE [37]. While the long-term cycling performance (Fig. 2) of graphite | sulfur cells with Li-Pyr showed similar SDCs, but lower C<sub>Eff</sub>s compared to graphite | AC cells[37], the SDCs and C<sub>Eff</sub>s of graphite | sulfur cells with Mg-Pyr are with only up to  $16 \pm 5$  mAh g<sup>-1</sup> and up to up to  $92.8 \pm 0.8\%$ in the 100<sup>th</sup> cycle notably lower compared their AC-based counterpart [37] ( $\approx 34 \pm 4 \text{ mAh g}^{-1}$ , up to  $99.8 \pm 0.1\%$ Fig. S8a and Table S3). The main origin of this poor SDCs is based on the high overpotential of the CE during discharge, respectively delithiation (Fig. S8b). During charge, TFSI<sup>-</sup>-intercalation above 4.7 V vs. LilLi<sup>+</sup> (WE) is in good agreement with previous potentials in graphite | AC cells [37]. Also the potential plateau of the CE at  $\approx 2.3$  to 2.4 V vs. LilLi<sup>+</sup> during lithiation indicates no notable overpotentials in comparison to the Li-Pyr-based cells. Nevertheless, even in the first discharge step, the potential limit of 3.1 V vs. LilLi<sup>+</sup> (CE) is reached after a steep potential increase and less than  $12.6 \pm 0.7$  mAh g<sup>-1</sup> with is only  $\approx 15\%$  of the charge capacity. According to the electron and ion inventory model [72], this is accompanied by remaining TFSI<sup>-</sup> in the WE, why even the charge capacities in the following cycles are low (<20 mAh g<sup>-1</sup>). This confirms literature results which indicate higher overpotentials especially for sulfur species oxidation in Mg<sup>2+</sup>-based electrolytes compared to Li<sup>+</sup>-based ones [76]. To the best of our knowledge, however, this was not yet observed for sulfur electrodes cycled with electrolytes of Mg-based salts in ILs.

If the potential of the CE is not limited and overpotentials of sulfur-species oxidation are not influencing the cycling performance of the WE (by the electron and ion inventory effect [72]), potential profiles and SDCs of graphite | sulfur cells are comparable to the ones of graphite | AC cells [37] (Fig. 6 and Table S3, up to  $36 \pm 2$  mAh g<sup>-1</sup>). Even the  $C_{\text{Eff}}$  is higher compared to graphite | sulfur cells with potential limits of the CE. The potentials of the (not limited) CE (Fig. 6b) show a clear plateau at  $\approx 3.15 \text{ V } vs. \text{ LilLi}^+ \text{ during the first}$ discharge, confirming that the cut-off potential of the CE used in this study (3.1 V vs. LilLi<sup>+</sup>) was too low to allow for sulfur-species re-oxidation. In later cycles (and at higher currents), however, no clear plateaus are visible, indicating sluggish kinetics at higher current densities. A larger amount of re-oxidized sulfur species might also be the origin of the increased C<sub>Eff</sub>s compared to the cells with potential limited CE, since less sulfur species are dissolved in the electrolyte. Still, similar to graphite | sulfur cells with Li-Pyr, increasing overpotentials of the CE during charge indicate electrode aging and loss of active material (sulfur). Similar to the WE cycled with Li-Pyr in a graphite | sulfur cell, the WE cycled with Mg-Pyr show slight morphology changes after cycling in graphite | sulfur, which are not obtained

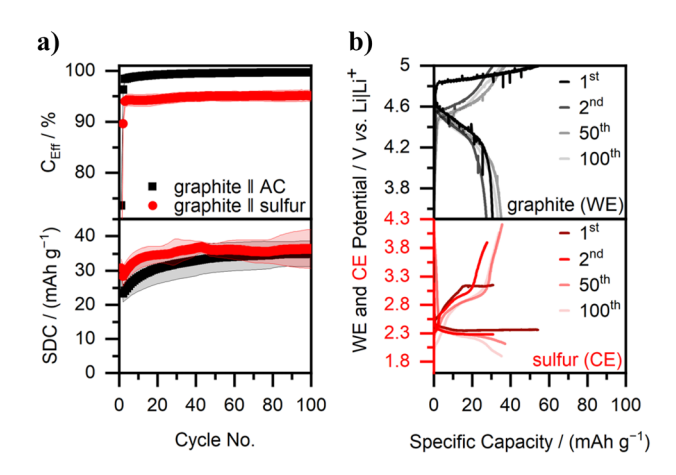


**Fig. 6.** a  $C_{Eff}$ s and SDCs of graphite  $\|$  sulfur (WE  $\|$  CE; red) and graphite  $\|$  AC (WE  $\|$  CE; black, data taken from ref. [37], published under the terms of a CC BY 4.0 license, https://creativecommons.org/licenses/by/4.0/) Swagelok-type cells (three-electrode configuration, half-cell setup) with 0.5 M Mg(TFSI)<sub>2</sub> in Pyr<sub>14</sub>TFSI (Mg-Pyr) electrolyte and a Li metal (Li|Li<sup>+</sup>) qRE at 20 °C, 100 mA g<sup>-1</sup> (10 mA g<sup>-1</sup> in the 1<sup>st</sup> cycle) and cut-off potentials of 3.4 and 5.0 V vs. Li|Li<sup>+</sup> for the WE. The potentials of the CEs were not limited. **b** The corresponding potential profiles of the WE (graphite, black) and CE (sulfur, red) at the 1<sup>st</sup>, 2<sup>nd</sup>, 50<sup>th</sup> and 100<sup>th</sup> cycle. The  $C_{Eff}$ s of the first cycle (CE=AC:  $74\pm1\%$  [37]; CE=sulfur:  $54\pm3\%$ ) are not shown.



in graphite | AC cells (Fig. S9a, b). Furthermore, the F:S ratio (Table S2) on the WEs indicates a sulfur-rich layer after cycling in graphite | sulfur cells (1.4:1) in comparison to a fluorine-rich layer after cycling in graphite | AC cells (3.7:1). The sulfur CE cycled with Mg-Pyr shows hollow structures on the surface (Fig. S9) and a reduced sulfur content after cycling (Table S2), as the ones cycled with Li-Pyr (Fig. S3c and Table S1).

Graphite  $\|$  sulfur full-cells with Mg-Pyr (Fig. S10) deliver SDCs up to  $\approx$ 22 mAh g $^{-1}$  and average discharge voltages up to 1.7 V ( $\approx$ 37 Wh kg $^{-1}$ ) but show capacity fading and high overpotentials during cycling, similar to the cells with Li-Pyr (Fig. S5).

In summary, these results show that, despite higher overpotentials especially for the sulfur-species oxidation, it is also possible to enable a graphite  $\mathbb{I}$  sulfur cell with Mg-ion-based electrolytes. Thereby, we present a transition metal-and Li-free battery cell, based on potentially sustainable active materials [19, 23]. Similar to MSBs, however, finding countermeasures for the high overpotentials of sulfur-based electrodes are key to improve their performance.

#### **Conclusion**

This work presents a transition-metal- and potentially Lifree energy storage concept based on an anion-intercalating graphite positive electrode and an elemental sulfur-based negative electrode. A stable cycling performance for 100 cycles of graphite | sulfur cells containing 1 M LiTFSI in Pyr<sub>14</sub>TFSI, but also 0.5 M Mg(TFSI)<sub>2</sub> Pyr<sub>14</sub>TFSI with specific discharge capacities over 30 mAh g<sup>-1</sup> could be demonstrated. Over long-term cycling, however, alteration of the sulfur-based negative electrode, likely based on active material loss was observed and led to decreased capacities in later cycles. Transport and subsequent reduction of dissolved PS on the WE were assumed to be the main cause for this and reduced the C<sub>Eff</sub>s in comparison to sulfur-free systems. Reduced C<sub>Eff</sub>s (below 70%) and alteration of the sulfur electrode were even more pronounced at low specific currents and elevated temperatures, albeit the kinetic hindrances and the overpotentials could be reduced.

Especially, for cells with Mg-ion-based electrolytes, the overpotentials of the sulfur-based electrode were higher in comparison to the Li-ion-based systems, and this is in good agreement with previous reports [76]. However, adjustment of the cut-off potentials of the sulfur-based electrode further allowed for an increase in the capacity retention and allowed a stable cycling.

To further improve this system and make it more competitive to state-of-the-art batteries, higher practical capacities are needed, for example by the adjustment of electrolyte and cut-off potentials. Furthermore, reduction of the

overpotentials at the sulfur-based electrode (especially for the Mg-ion-based system), but also limited transport of dissolved sulfur species, *e.g.* by sulfur trapping close to the electrode, are needed to improve the cycling performance. Hereby, for example modifications of the sulfur-composite electrode [30, 79] or the separator [80, 81], but also the application of SPAN [13–16] are possible. In addition, a high impact of the electrolyte solvent on the overpotential for sulfur reduction and oxidation was observed [76], indicating that the electrolyte needs further and careful attention. Furthermore, the application of electrolytes with cations beyond Li<sup>+</sup> and Mg<sup>2+</sup> such as Na<sup>+</sup> might as well as allow for cells with highly abundant elements.

## **Experimental section**

#### Electrodes, electrolytes and cell assembly

The positive graphite-based electrodes (P; here: working electrode; WE) were prepared from an aqueous solution with solid components consisting of 90 wt.% KS6 graphite (Imerys Graphite & Carbon), 5 wt.% Super C65 carbon black (Imerys Graphite & Carbon) and 5 wt.% sodium carboxymethyl cellulose (CMC) binder (Sigma Aldrich, Mw  $\approx$ 90,000), casted on aluminum foil (Goodfellow, 20 µm) as described in detail in previous works [37, 74]. The average active mass loading was  $1.9 \pm 0.2$  mg cm<sup>-2</sup> on 12 mm circular electrodes. Activated carbon (AC)-based electrodes consisted of 85 wt.% AC (Norit), 5 wt.% PTFE (60 wt.% in aqueous solution; Sigma Aldrich) and 10 wt.% Super C65 and were processed as described before [37].

In order to process the sulfur-based negative electrodes (N; here: counter electrode; CE), elemental sulfur (Sigma Aldrich, 99.998%) and the carbon black (CB) Ensaco 250 (Imerys Graphite & Carbon) were dry-mixed in a ratio of 2:1 for 10 h in a ball mill (Fritsch, Pulverisette 7) with 250 rpm. The sulfur/CB mixture was mortared and mixed in a ball mill (2 h, 250 rpm) with a solid weight ratio of 80:10:10 with Ketjenblack® EC 600JD (Akzo Nobel) and a 2 wt.% aqueous sodium alginate solution (Sigma Aldrich). The electrode paste was then coated with a doctor blade on a carbon-coated aluminum foil and dried at 60 °C for one hour. The electrodes with a diameter of 12 mm were further dried at 50 °C *in vacuo* overnight and active material loadings (sulfur) of 0.65 ± 0.05 cm<sup>-2</sup> were obtained.

The electrolytes (Li-Pry, respectively Mg-Pyr) were prepared by mixing 1 M lithium bis (trifluoromethanesulfonyl) imide (LiTFSI; Solvionic, 99.9%) or 0.5 M magnesium bis (trifluoromethanesulfonyl)imide (Mg(TFSI)<sub>2</sub>; Solvionic, 99.5%) with 1-butyl-1-methylpyrrolidinium bis (trifluoromethanesulfonyl)imide (Pyr<sub>14</sub>TFSI, Solvionic, 99.9%) at 60 °C, after drying the components *in vacuo* at 110 °C for 24 h.



Charge/discharge cycling was performed in Swagelok-type cells (3-electrode configuration) in a half-cell setup (= control of WE potential via the reference electrode). In this cell setup, graphite composite electrodes were used as WE (each 12 mm), AC- [37] or sulfur-based composite electrodes as CE (12 mm) and Li metal as (quasi) reference electrode ((q)RE; 5 mm). In all cells, two 13 mm and two 10 mm Whatman GF/A separators soaked with  $170+50~\mu L$  electrolyte were used for separation of the WE from the CE and RE, respectively. Graphite | sulfur cells additionally contained a Celgard 2500 separator (13 mm) with  $10~\mu L$  electrolyte facing the CE.

Dried electrolytes and electrodes were stored and cells were built in a dry room with water contents below 0.02% (for graphite | AC cells) [37] or under argon atmosphere in a glovebox with water and oxygen values below 5 ppm (for graphite | sulfur cells).

### **Electrochemical investigations**

All electrochemical investigations of graphite | AC [37] cells were performed at 20 °C on a MACCOR Series 4000 battery cycler (MACCOR INC.), while graphite | sulfur cells were cycled using a multi-channel potentiostat (VMP3, BioLogic) at 20 °C or 60 °C.

For long-term cycling, a three-electrode setup with a Li metal (q)RE was cycled at a specific current of 100 mA g<sup>-1</sup> (1<sup>st</sup> cycle: 10 mA g<sup>-1</sup>) and controlled WE potentials with cut-off potentials of 3.4 to 4.9 V vs. LilLi<sup>+</sup> (with Li-Pyr), respectively 5.0 V vs. LilLi<sup>+</sup> (with Mg-Pyr) for the WE. The CE potential of graphite | sulfur cells was additionally limited to 1.5 to 3.0 V vs. LilLi<sup>+</sup> (with Li-Pyr), respectively 1.6 to 3.1 V vs. LilLi<sup>+</sup> (with Mg-Pyr), if not stated otherwise. This setup was chosen to determine the effects of the WE and CE, separately. In order to evaluate the performance at different specific currents, after one pre-cycle at 10 mA g<sup>-1</sup> and 30 cycles at 100 mA g<sup>-1</sup>, different currents from 10 to 1000 mA g<sup>-1</sup> with five cycles per current were applied. The cut-off potentials were identical to the ones of long-term cycling investigations (with controlled WE and limited CE potentials for graphite | sulfur cells). The SDCs and C<sub>Eff</sub>s of the 5<sup>th</sup> cycle of each current are displayed. A more detailed description of the cycling procedures is given in Küpers et al. [37]. In order determine the reproducibility, at least three identical cells were built for each investigation, and deviations are indicated by error bars.

### X-ray diffraction

Ex situ X-ray diffraction measurements of pristine and cycled graphite electrodes were performed at room temperature between

 $20^{\circ}$  and  $35^{\circ}$  (step sizes of  $0.02^{\circ}$ ) on a Bruker D8 Advance diffractometer with Cu K $\alpha$  radiation (1.54 Å). The samples were placed on a single crystal silicon sample holder and fixed with Kapton foil. Analysis and background subtraction were performed with the Diffrac.Eva 3.1 (Bruker) software.

Prior to measurements, the graphite electrodes were cycled three full cycles and one charge to 4.9 V, respectively 5.0 V vs. LilLi<sup>+</sup> at 10 mA g<sup>-1</sup>. Cut-off potentials were equal to the ones described above. The cells were disassembled under argon atmosphere (for graphite  $\parallel$  sulfur cells) or ambient air (graphite  $\parallel$  AC cells) [37] and measured without a washing procedure.

# Scanning electron microscopy and energy-dispersive x-ray spectroscopy

A scanning electron microscope (Carl Zeiss Microscopy GmbH, Schottky field emission gun) was used to investigate the surface morphology of pristine and cycled electrodes. All images were obtained at a working distance of 5 mm using an acceleration voltage of 3 kV and an in-lens secondary electron detector. EDX spectra were obtained at an acceleration voltage of 15 kV with an EDX detector (X-Max 80 mm², Oxford Instruments). Prior to the measurement, the samples were collected by disassembling the cells under argon atmosphere, and washing with 1 mL 1,2-Dimethoxyethane. The samples were transferred to the SEM device in an air tight sample holder.

**Supplementary information** The online version contains supplementary material available at https://doi.org/10.1007/s10008-022-05215-w.

**Acknowledgements** Generous support by the German Federal Ministry of Education and Research (BMBF) within the projects 'MgMeAnS' (03XP0140) and 'MvBIC' (03XP0249) is gratefully acknowledged.

Author contributions Verena Küpers: Conceptualization, Formal analysis, Investigation, Writing—Original Draft, Visualization. Martin Kolek: Conceptualization, Writing—Review & Editing, Supervision. Peter Bieker: Writing—Review & Editing, Supervision. Marian Stan: Writing—Review & Editing, Supervision. Tobias Placke: Writing—Review & Editing, Supervision. Martin Winter: Conceptualization, Writing—Review & Editing, Supervision, Project administration, Funding acquisition.

Funding Open Access funding enabled and organized by Projekt DEAL.

Open Access This article is licensed under a Creative Commons Attribution 4.0 International License, which permits use, sharing, adaptation, distribution and reproduction in any medium or format, as long as you give appropriate credit to the original author(s) and the source, provide a link to the Creative Commons licence, and indicate if changes were made. The images or other third party material in this article are included in the article's Creative Commons licence, unless indicated otherwise in a credit line to the material. If material is not included in the article's Creative Commons licence and your intended use is not permitted by statutory regulation or exceeds the permitted use, you will need to obtain permission directly from the copyright holder. To view a copy of this licence, visit <a href="http://creativecommons.org/licenses/by/4.0/">http://creativecommons.org/licenses/by/4.0/</a>.



#### References

- European Commission, Directorate-General for Internal Market, Industry, Entrepreneurship and SMEs (2020) Communication from the commission to the European parliament, the council, the European economic and social committee and the committee of the regions, Critical raw materials resilience: Charting a path towards greater security and sustainability. https://eur-lex.europa.eu/legal-content/EN/TXT/?uri=CELEX:52020DC0474. Accessed April 2022
- Olivetti EA, Ceder G, Gaustad GG, Fu X (2017) Lithium-ion battery supply chain considerations: Analysis of potential bottlenecks in critical metals. Joule 1:229–243
- Dühnen S, Betz J, Kolek M, Schmuch R, Winter M, Placke T (2020) Toward green battery cells: Perspective on materials and technologies. Small Methods 4:2000039
- Greim P, Solomon AA, Breyer C (2020) Assessment of lithium criticality in the global energy transition and addressing policy gaps in transportation. Nat Comm 11:4570
- Wentker M, Greenwood M, Asaba MC, Leker J (2019) A raw material criticality and environmental impact assessment of state-of-the-art and post-lithium-ion cathode technologies. J Energy Stor 26:101022
- Bieker G, Küpers V, Kolek M, Winter M (2021) Intrinsic differences and realistic perspectives of lithium-sulfur and magnesium-sulfur batteries. Commun Mater 2:37
- Dörfler S, Walus S, Locke J, Fotouhi A, Auger DJ, Shateri N, Abendroth T, Härtel P, Althues H, Kaskel S (2021) Recent progress and emerging application areas for lithium-sulfur battery technology. Energ Technol 9:2000694
- 8. Rosenman A, Markevich E, Salitra G, Aurbach D, Garsuch A, Chesneau FF (2015) Review on Li-sulfur battery systems: an integral perspective. Adv Energy Mater 5:1500212
- Zhao H, Deng N, Yan J, Kang W, Ju J, Ruan Y, Wang X, Zhuang X, Li Q, Cheng B (2018) A review on anode for lithium-sulfur batteries: Progress and prospects. Chem Eng J 347:343–365
- Zhao M, Li B-Q, Peng H-J, Yuan H, Wei J-Y, Huang J-Q (2020) Lithium-sulfur batteries under lean electrolyte conditions: challenges and opportunities. Angew Chem Int Ed 59:12636–12652
- Yang C, Suo L, Borodin O, Wang F, Sun W, Gao T, Fan X, Hou S, Ma Z, Amine K, Xu K, Wang C (2017) Unique aqueous Li-ion/ sulfur chemistry with high energy density and reversibility. Proc Natl Acad Sci USA 114:6197–6202
- Kumar M, Nagaiah TC (2022) A unique 2.1 V "water in salt" elemental sulfur based Na-ion hybrid storage capacitor. https://doi.org/10.1039/D1TA10940E
- Berhe GB, Su W-N, Huang C-J, Hagos TM, Hagos TT, Bezabh HK, Weret MA, Abrha LH, Yang Y-W, Hwang B-J (2019) A new class of lithium-ion battery using sulfurized carbon anode from polyacrylonitrile and lithium manganese oxide cathode. J Power Sources 434:126641
- 14. Berhe GB, Su W-N, Abrha LH, Bezabh HK, Hagos TM, Hagos TT, Huang C-J, Sahalie NA, Jote BA, Thirumalraj B, Kurniawan D, Wang C-H, Hwang BJ (2020) Garnet–PVDF composite film modified lithium manganese oxide cathode and sulfurized carbon anode from polyacrylonitrile for lithium-ion batteries. J Mater Chem A 8:14043–14053
- Wu Y, Wang W, Ming J, Li M, Xie L, He X, Wang J, Liang S, Wu Y (2019) An exploration of new energy storage system: High energy density, high safety, and fast charging lithium ion battery. Adv Funct Mater 29:1805978
- Shuai Y, He X, Zhang Z, Chen K, Lou J, Wang Y, Li N (2019) A
  Highly reversible and low-cost sulfur-graphite dual-ion battery.
  Energ Technol 7:1800729
- Andre D, Kim S-J, Lamp P, Lux SF, Maglia F, Paschos O, Stiaszny B (2015) Future generations of cathode materials: an automotive industry perspective. J Mater Chem A 3:6709–6732

- U.S. Department of the Interior, U.S. Geological Survey (2022) Mineral commodity summaries. https://www.usgs.gov/centers/nmic/mineralcommodity-summaries. Accessed April 2022
- Liedel C (2020) Sustainable Battery Materials from Biomass. Chemsuschem 13:2110–2141
- Winter M, Kolek M, Bieker P, Küpers V (2020) Electrochemical cell with sulfur electrode and reversible dual-ion charge transfer. Publication date 2021-07-15, Patent No. DE102020108397
- Nölle R, Beltrop K, Holtstiege F, Kasnatscheew J, Placke T, Winter M (2019) A reality check and tutorial on electrochemical characterization of battery cell materials: How to choose the appropriate cell setup. Mater Today 32:131–146
- Betz J, Bieker G, Meister P, Placke T, Winter M, Schmuch R (2019) Theoretical versus practical energy: A plea for more transparency in the energy calculation of different rechargeable battery systems. Adv Energy Mater 9:1803170
- Placke T, Heckmann A, Schmuch R, Meister P, Beltrop K, Winter M (2018) Perspective on performance, cost, and technical challenges for practical dual-ion batteries. Joule 2:2528–2550
- 24. Gröbmeyer A, Becking J, Bieker PM, Winter M, Stan MC (2019) A Facile preparation of S8/C composite cathode for lithium-sulfur cells: influence of intrinsic and extrinsic cathode properties on the electrochemical performance. Energ Technol 7:1800789
- Park J-W, Ueno K, Tachikawa N, Dokko K, Watanabe M (2013) Ionic liquid electrolytes for lithium-sulfur batteries. J Phys Chem C 117:20531–20541
- Salama M, Rosy AR, Yemini R, Gofer Y, Aurbach D, Noked M (2019) Metal-sulfur batteries: Overview and research methods. ACS Energy Lett 4:436–446
- Xu K (2004) Nonaqueous liquid electrolytes for lithium-based rechargeable batteries. Chem Rev 104:4303–4418
- Cekic-Laskovic I, von Aspern N, Imholt L, Kaymaksiz S, Oldiges K, Rad BR, Winter M (2019) Synergistic Effect of Blended Components in Nonaqueous Electrolytes for Lithium Ion Batteries. In: Eichel R-A (ed) Electrochemical Energy Storage: Next Generation Battery Concepts. Springer International Publishing, Cham, pp 1–64
- Gao J, Lowe MA, Kiya Y, Abruña HD (2011) Effects of liquid electrolytes on the charge-discharge performance of rechargeable lithium/sulfur batteries: Electrochemical and in-situ x-ray absorption spectroscopic studies. J Phys Chem C 115:25132–25137
- Zhang S, Ueno K, Dokko K, Watanabe M (2015) Recent advances in electrolytes for lithium-sulfur batteries. Adv Energy Mater 5:1500117
- 31. Beltrop K, Meister P, Klein S, Heckmann A, Grünebaum M, Wiemhöfer H-D, Winter M, Placke T (2016) Does size really matter? New insights into the intercalation behavior of anions into a graphite-based positive electrode for dual-ion batteries. Electrochim Acta 209:44–55
- Rothermel S, Meister P, Schmuelling G, Fromm O, Meyer H-W, Nowak S, Winter M, Placke T (2014) Dual-graphite cells based on the reversible intercalation of bis(trifluoromethanesulfonyl) imide anions from an ionic liquid electrolyte. Energy Environ Sci 7:3412–3423
- Schmuelling G, Placke T, Kloepsch R, Fromm O, Meyer H-W, Passerini S, Winter M (2013) X-ray diffraction studies of the electrochemical intercalation of bis(trifluoromethanesulfonyl) imide anions into graphite for dual-ion cells. J Power Sources 239:563–571
- Placke T, Fromm O, Lux SF, Bieker P, Rothermel S, Meyer H-W, Passerini S, Winter M (2012) Reversible intercalation of Bis(trifluoromethanesulfonyl)imide anions from an ionic liquid electrolyte into graphite for high performance dual-ion Cells. J Electrochem Soc 159:A1755–A1765
- Liu Y, Elias Y, Meng J, Aurbach D, Zou R, Xia D, Pang Q (2021) Electrolyte solutions design for lithium-sulfur batteries. Joule 5:2323–2364



- Li G, Wang S, Zhang Y, Li M, Chen Z, Lu J (2018) Revisiting the Role of polysulfides in lithium-sulfur batteries. Adv Mater 30:1705590
- Küpers V, Dohmann JF, Bieker P, Winter M, Placke T, Kolek M (2021) Opportunities and limitations of ionic liquid- and organic carbonate solvent-based electrolytes for Mg-ion-based dual-ion batteries. Chemsuschem 14:4480–4498
- Meister P, Fromm O, Rothermel S, Kasnatscheew J, Winter M, Placke T (2017) Sodium-based vs. lithium-based dual-ion cells: electrochemical study of anion intercalation/de-intercalation into/from graphite and metal plating/dissolution behavior. Electrochim Acta 228:18–27
- Beltrop K, Beuker S, Heckmann A, Winter M, Placke T (2017)
   Alternative electrochemical energy storage: potassium-based dual-graphite batteries. Energy Environ Sci 10:2090–2094
- Lei X, Zheng Y, Zhang F, Wang Y, Tang Y (2020) Highly stable magnesium-ion-based dual-ion batteries based on insoluble small-molecule organic anode material. Energy Storage Mater 30:34–41
- Yang R, Zhang F, Lei X, Zheng Y, Zhao G, Tang Y, Lee C-S (2020) Pseudocapacitive Ti-doped niobium pentoxide nanoflake structure design for a fast kinetics anode toward a highperformance Mg-ion-based dual-ion battery. ACS Appl Mater Interfaces 12:47539–47547
- Meister P, Küpers V, Kolek M, Kasnatscheew J, Pohlmann S, Winter M, Placke T (2021) Enabling Mg-based ionic liquid electrolytes for hybrid dual-ion capacitors. Batter Supercaps 4:504–512
- 43. Wu S, Zhang F, Tang Y (2018) A novel calcium-ion battery based on dual-carbon configuration with high working voltage and long cycling life. Adv Sci Lett 5(8):1701082
- Yu X, Manthiram A (2020) A Progress report on metal-sulfur batteries. Adv Funct Mater 30:2004084
- 45. Hans Wedepohl K (1995) The composition of the continental crust. Geochim Cosmochim Acta 59:1217–1232
- Zhang Y, Geng H, Wei W, Ma J, Chen L, Li CC (2019) Challenges and recent progress in the design of advanced electrode materials for rechargeable Mg batteries. Energy Storage Mater 20:118–138
- Liang Y, Dong H, Aurbach D, Yao Y (2020) Current status and future directions of multivalent metal-ion batteries. Nat Energy 5:646–656
- Yoo HD, Shterenberg I, Gofer Y, Gershinsky G, Pour N, Aurbach D (2013) Mg rechargeable batteries: an on-going challenge. Energy Environ Sci 6:2265–2279
- Shterenberg I, Salama M, Gofer Y, Levi E, Aurbach D (2014) The challenge of developing rechargeable magnesium batteries. MRS Bull 39:453

  –460
- Muldoon J, Bucur CB, Gregory T (2014) Quest for nonaqueous multivalent secondary batteries: Magnesium and beyond. Chem Rev 114:11683–11720
- Matsui M (2011) Study on electrochemically deposited Mg metal.
   J Power Sources 196:7048–7055
- 52. Gregory TD (1990) Nonaqueous electrochemistry of magnesium. J Electrochem Soc 137:775
- Fichtner M (2020) Magnesium Batteries: Research and Applications. R Soc Chem
- Aurbach D, Lu Z, Schechter A, Gofer Y, Gizbar H, Turgeman R, Cohen Y, Moshkovich M, Levi E (2000) Prototype systems for rechargeable magnesium batteries. Nature 407:724
- Dominko R, Bitenc J, Berthelot R, Gauthier M, Pagot G, Di Noto V (2020) Magnesium batteries: Current picture and missing pieces of the puzzle. J Power Sources 478:229027
- Salama M, Attias R, Hirsch B, Yemini R, Gofer Y, Noked M, Aurbach D (2018) On the feasibility of practical Mg–S batteries: Practical limitations associated with metallic magnesium anodes. ACS Appl Mater Interfaces 10:36910–36917

- Kim HS, Arthur TS, Allred GD, Zajicek J, Newman JG, Rodnyansky AE, Oliver AG, Boggess WC, Muldoon J (2011) Structure and compatibility of a magnesium electrolyte with a sulphur cathode. Nat Comm 2:427
- Shi J, Zhang J, Guo J, Lu J (2020) Interfaces in rechargeable magnesium batteries. Nanoscale Horizons 5:1467–1475
- Liu F, Wang T, Liu X, Fan L-Z (2021) Challenges and recent progress on key materials for rechargeable magnesium batteries. Adv Energy Mater 11:2000787
- Placke T, Bieker P, Lux Simon F, Fromm O, Meyer H-W, Passerini S, Winter M (2012) Dual-ion cells based on anion intercalation into graphite from ionic liquid-based electrolytes. Z Phys Chem 226:391
- 61. Zhao-Karger Z, Zhao X, Wang D, Diemant T, Behm RJ, Fichtner M (2015) Performance improvement of magnesium sulfur batteries with modified non-nucleophilic electrolytes. Adv Energy Mater 5:1401155
- Cheek GT, O'Grady WE, El Abedin SZ, Moustafa EM, Endres F (2008) Studies on the Electrodeposition of magnesium in ionic liquids. J Electrochem Soc 155:D91–D95
- Amir N, Vestfrid Y, Chusid O, Gofer Y, Aurbach D (2007) Progress in nonaqueous magnesium electrochemistry. J Power Sources 174:1234–1240
- Vardar G, Sleightholme AES, Naruse J, Hiramatsu H, Siegel DJ, Monroe CW (2014) Electrochemistry of magnesium electrolytes in ionic liquids for secondary batteries. ACS Appl Mater Interfaces 6:18033–18039
- Watkins T, Kumar A, Buttry DA (2016) Designer ionic liquids for reversible electrochemical deposition/dissolution of magnesium. J Am Chem Soc 138:641–650
- Gao X, Mariani A, Jeong S, Liu X, Dou X, Ding M, Moretti A, Passerini S (2019) Prototype rechargeable magnesium batteries using ionic liquid electrolytes. J Power Sources 423:52–59
- 67. Yan J, Liu X, Li B (2016) Capacity fade analysis of sulfur cathodes in lithium-sulfur batteries. Adv Sci Lett 3:1600101
- Bieker G, Wellmann J, Kolek M, Jalkanen K, Winter M, Bieker P (2017) Influence of cations in lithium and magnesium polysulphide solutions: dependence of the solvent chemistry. Phys Chem Chem Phys 19:11152–11162
- Kotronia A, Asfaw HD, Tai C-W, Hahlin M, Brandell D, Edström K (2021) Nature of the cathode-electrolyte interface in highly concentrated electrolytes used in graphite dual-ion batteries. ACS Appl Mater Interfaces 13:3867–3880
- Wang GX, Ahn J-H, Lindsay MJ, Sun L, Bradhurst DH, Dou SX, Liu HK (2001) Graphite-Tin composites as anode materials for lithium-ion batteries. J Power Sources 97–98:211–215
- Park J-W, Yamauchi K, Takashima E, Tachikawa N, Ueno K, Dokko K, Watanabe M (2013) Solvent effect of room temperature ionic liquids on electrochemical reactions in lithium-sulfur batteries. J Phys Chem C 117:4431–4440
- Heidrich B, Heckmann A, Beltrop K, Winter M, Placke T (2019) Unraveling charge/discharge and capacity fading mechanisms in dual-graphite battery cells using an electron inventory model. Energy Storage Mater 21:414

  –426
- Reddy TB (2011) Linden's Handbook of Batteries, 4th edn. New York, USA, McGraw-Hill Education
- 74. Placke T, Rothermel S, Fromm O, Meister P, Lux SF, Huesker J, Meyer H-W, Winter M (2013) Influence of graphite characteristics on the electrochemical intercalation of Bis(trifluoromethanesulfonyl) imide anions into a graphitebased cathode. J Electrochem Soc 160:A1979–A1991
- Heckmann A, Meister P, Kuo L-Y, Winter M, Kaghazchi P, Placke T (2018) A route towards understanding the kinetic processes of bis(trifluoromethanesulfonyl) imide anion intercalation into graphite for dual-ion batteries. Electrochim Acta 284:669–680



- Bieker G, Diddens D, Kolek M, Borodin O, Winter M, Bieker P, Jalkanen K (2018) Cation-dependent electrochemistry of polysulfides in lithium and magnesium electrolyte solutions. J Phys Chem C 122:21770–21783
- Heckmann A, Thienenkamp J, Beltrop K, Winter M, Brunklaus G, Placke T (2018) Towards high-performance dual-graphite batteries using highly concentrated organic electrolytes. Electrochim Acta 260:514–525
- Münster P, Heckmann A, Nölle R, Winter M, Beltrop K, Placke T (2019) Enabling high performance potassium-based dual-graphite battery cells by highly concentrated electrolytes. Batter Supercaps 2:992–1006
- Yu X, Manthiram A (2016) Performance enhancement and mechanistic studies of magnesium-sulfur cells with an advanced cathode structure. ACS Energy Lett 1:431–437

- 80. Ford HO, Merrill LC, He P, Upadhyay SP, Schaefer JL (2018) Cross-linked ionomer gel separators for polysulfide shuttle mitigation in magnesium-sulfur batteries: elucidation of structure-property relationships. Macromolecules 51:8629–8636
- Manthiram A, Fu Y, Chung S-H, Zu C, Su Y-S (2014) Rechargeable Lithium-Sulfur Batteries. Chem Rev 114:11751–11787
- Gao T, Hou S, Wang F, Ma Z, Li X, Xu K, Wang C (2017) Reversible S<sup>0</sup>/MgS<sub>x</sub> redox chemistry in a MgTFSI<sub>2</sub>/MgCl<sub>2</sub>/DME electrolyte for rechargeable Mg/S batteries. Angew Chem Int Ed 56:13526–13530

**Publisher's Note** Springer Nature remains neutral with regard to jurisdictional claims in published maps and institutional affiliations.

